Observation of trapped light within the radiation continuum

Observation of trapped light within the radiation continuum

Chia Wei Hsu[1,2*], Bo Zhen[1*], Jeongwon Lee[1], Song-Liang Chua[1], Steven G. Johnson[1,3], John D. Joannopoulos[1] & Marin Soljačić[1]

[1]Research Laboratory of Electronics, Massachusetts Institute of Technology, Cambridge, Massachusetts 02139, USA.

[2]Department of Physics, Harvard University, Cambridge, Massachusetts 02138, USA.

[3]Department of Mathematics, Massachusetts Institute of Technology, Cambridge, Massachusetts 02139, USA.

*These authors contributed equally to this work.

The ability to confine light is important both scientifically and technologically. Many light confinement methods exist, but they all achieve confinement with materials or systems that forbid outgoing waves. Such systems can be implemented by metallic mirrors, by photonic band-gap materials[1], by highly disordered media (Anderson localization[2]) and, for a subset of outgoing waves, by translational symmetry (total internal reflection[1]) or rotation/reflection symmetry[3,4]. Exceptions to these examples exist only in theoretical proposals[5–8]. Here we predict and experimentally demonstrate that light can be perfectly confined in a patterned dielectric slab, even though outgoing waves are allowed in the surrounding medium. Technically, this is an observation of an "embedded eigenvalue"[9]—namely a bound state in a continuum of radiation modes—that is not due to symmetry incompatibility[5–8,10–16]. Such a bound

state can exist stably in a general class of geometries where all of its radiation amplitudes vanish simultaneously due to destructive interference. This method to trap electromagnetic waves is also applicable to electronic[12] and mechanical waves[14,15].

The propagation of waves can be easily understood from the wave equation, but the localization of waves (creation of bound states) is more complex. Typically, wave localization can only be achieved when suitable outgoing waves either do not exist or are forbidden due to symmetry incompatibility. For electromagnetic waves, this is commonly implemented with metals, photonic bandgaps, or total internal reflections; for electron waves, this is commonly achieved with potential barriers. In 1929, von Neumann and Wigner proposed the first counterexample[10], in which they designed a quantum potential to trap an electron whose energy would normally allow coupling to outgoing waves. However, such artificially designed potential does not exist in reality. Furthermore, the trapping is destroyed by any generic perturbation to the potential. More recently, other counterexamples have been proposed theoretically in quantum systems[11–13], photonics[5–8], acoustic and water waves[14,15], and mathematics[16]; the proposed systems in refs. 6 and 14 are most closely related to what is demonstrated here. While no general explanation exists, some cases have been interpreted as two interfering resonances that leaves one resonance with zero width[6,11,12]. Among these many proposals, most cannot be readily realized due to their inherent fragility. A different form of embedded eigenvalue has been realized in symmetry-protected systems[3,4], where no outgoing wave exists for modes of a particular symmetry.

To show that an optical bound state is feasible even when it is surrounded by symmetry-compatible radiation modes, we consider a practical structure: a dielectric slab with a square array

of cylindrical holes (Fig. 1a), an example of photonic crystal (PhC) slab[1]. The periodic geometry leads to photonic band structures, analogous to how a periodic potential in solids gives rise to electron band structures. The PhC slab supports guided resonances whose frequencies lie within the continuum of radiation modes in free space (Fig. 1b); these resonances generally have finite lifetimes because they can couple to the free-space modes. However, using finite-difference time-domain (FDTD) simulations[17] and along with the analytical proof below, we find that the lifetime of the resonance goes to infinity at discrete k points on certain bands; here we focus on the lowest TM-like band in the continuum (referred to as TM_1 hereafter), with its lifetime shown in Fig. 1c, d. At these seemingly unremarkable k points, light becomes perfectly confined in the slab, as is evident both from the divergent lifetime and from the field profile (Fig. 1e). These states are no longer leaky resonances; they are eigenmodes that do not decay. In the functional analysis literature, eigenvalues like this, which exist within the continuous spectrum of radiation modes, are called *embedded eigenvalues*[9]. Here, embedded eigenvalues occur at five k points over the first Brillouin zone. The one at Γ arises because symmetry forbids coupling to any outgoing wave[4]; the other four (which are equivalent under 90° rotations) deserve further analysis since, intuitively, they should not be confined.

To understand this unexpected disappearance of leakage, we examine the outgoing planewaves. Using Bloch's theorem[1], we let the electric and magnetic fields of the resonance be $\mathbf{E}_\mathbf{k}(\boldsymbol{\rho}, z) = e^{i\mathbf{k}\cdot\boldsymbol{\rho}}\mathbf{u}_\mathbf{k}(\boldsymbol{\rho}, z)$ and $\mathbf{H}_\mathbf{k}(\boldsymbol{\rho}, z) = e^{i\mathbf{k}\cdot\boldsymbol{\rho}}\mathbf{v}_\mathbf{k}(\boldsymbol{\rho}, z)$ where $\mathbf{k} = (k_x, k_y, 0)$, and $\mathbf{u}_\mathbf{k}$, $\mathbf{v}_\mathbf{k}$ are periodic functions in $\boldsymbol{\rho} = (x, y)$. Outside of the slab, these fields are composed of planewaves that propagate energy and evanescent waves that decay exponentially. For frequencies below the diffraction limit,

the only propagating-wave amplitudes are the zeroth-order Fourier coefficients, given by

$$c_s(\mathbf{k}) = \langle \hat{\mathbf{e}}_\mathbf{k} \cdot \mathbf{u}_\mathbf{k} \rangle, \quad c_p(\mathbf{k}) = \langle \hat{\mathbf{e}}_\mathbf{k} \cdot \mathbf{v}_\mathbf{k} \rangle \tag{1}$$

for s and p polarizations respectively, where $\hat{\mathbf{e}}_\mathbf{k} = (k_y, -k_x, 0)/|\mathbf{k}|$ is the polarization direction of the in-plane fields, and the brackets denote spatial average on some x-y plane outside of the slab. The outgoing power from the resonance is proportional to $(|c_s|^2 + |c_p|^2)\cos\theta$, with θ being the angle of propagation. In general, c_s and c_p are two non-zero complex numbers, with a total of *four* degrees of freedom: therefore the outgoing power is unlikely to be zero when only two parameters (k_x and k_y) are varied.

However, for a certain class of geometries, the degrees of freedom can be reduced. If the structure has time-reversal symmetry $\epsilon(\mathbf{r}) = \epsilon^*(\mathbf{r})$ and inversion symmetry $\epsilon(\mathbf{r}) = \epsilon(-\mathbf{r})$, then the periodic part of the fields can be chosen to satisfy $\mathbf{u}_\mathbf{k}(\mathbf{r}) = \mathbf{u}^*_\mathbf{k}(-\mathbf{r})$ and $\mathbf{v}_\mathbf{k}(\mathbf{r}) = \mathbf{v}^*_\mathbf{k}(-\mathbf{r})$ (ref. 18). If the structure also has a mirror symmetry in z direction, then the fields must transform as ± 1 under mirror flips in z (ref. 1), so the plane-parallel components must satisfy $\mathbf{u}^\parallel_\mathbf{k}(x, y, z) = \pm\mathbf{u}^\parallel_\mathbf{k}(x, y, -z)$ and $\mathbf{v}^\parallel_\mathbf{k}(x, y, z) = \mp\mathbf{v}^\parallel_\mathbf{k}(x, y, -z)$. Following these two properties, the amplitudes c_s and c_p must be purely real or purely imaginary numbers on every k point. With only *two* degrees of freedom left, it may be possible that the two amplitudes cross zero simultaneously as two parameters k_x and k_y are scanned. A simultaneous crossing at zero means no outgoing power, and therefore, a perfectly confined state. We note that such an "accidental" crossing is distinct from those where leakage is forbidden due to symmetry incompatibility between the confined mode and the radiation modes[3,4].

This disappearance of leakage may also be understood as the destructive interference be-

tween several leakage channels. The field profile inside the PhC slab can be written as a superposition of waves with different propagation constants β_z in z direction. At the slab-medium interface, each wave partially reflects back into the slab, and partially transmits into the medium to become an outgoing planewave. The transmitted waves from different β_z channels interfere, and at appropriate k points they may cancel each other. One can make this argument quantitative by writing down the corresponding equations, yet because this argument ignores the existence of evanescent waves, it is intrinsically an approximation that works best for slabs much thicker than the wavelength[14]. Nonetheless, this argument provides an intuitive physical picture that supplements the exact (yet less intuitive) mathematical proof given above.

With FDTD simulations, we confirm that both Fourier amplitudes are zero at the k points where the special trapped state is observed (Fig. 1f, g). The zeros of c_s on the two axes and the zeros of c_p on the diagonal lines arise from symmetry mismatch, but the zeros of c_p along the roughly circular contour are "accidental" crossings that would not be meaningful if c_p had both real and imaginary parts. We have checked that a frequency-domain eigenmode solver[18] also predicts planewave amplitudes that cross zero at these k points. The trapped state is *robust*, because small variations of the system parameters (such as cylinder diameter) only move the crossing to a different value of k_x. This robustness is crucial for our experimental realization of such states. In fact, the trapped state persists even when the C_4 rotational symmetry of the structure is broken (Supplementary Fig. 1). However, perturbations that break inversion or mirror symmetry will introduce additional degrees of freedom in the Fourier amplitudes, thus reducing the infinite-lifetime bound state into a long-lived leaky resonance (Supplementary Fig. 2) unless additional tuning parameters

are used.

To experimentally confirm the existence of this trapped state, we use interference lithography to fabricate a macroscopic Si_3N_4 PhC slab ($n = 2.02$, thickness 180 nm) with a square array of cylindrical holes (periodicity 336 nm, hole diameter 160 nm), separated from the lossy silicon substrate with 6 μm of silica (Fig. 2a). Scanning electron microscope (SEM) images of the sample are shown in Fig. 2b, c. The material Si_3N_4 provides low absorption and enough index contrast with the silica layer ($n = 1.46$). To create an optically symmetric environment needed to reduce the degrees of freedom in the outgoing-wave amplitudes, we etch the holes through the entire Si_3N_4 layer, and immerse the sample in an optical liquid that is index-matched to silica. We perform angle-resolved reflectivity measurements (schematic setup shown in Fig. 2d) to characterize the PhC sample.

Light incident on the PhC slab excites the guided resonances, creating sharp Fano features in the reflectivity spectrum[19]. In comparison, a perfect bound state has no Fano feature, because it is decoupled from far-field radiation. In the measured reflectivity spectrum (Fig. 3a), we indeed observe that the Fano feature of the TM_1 band disappears near 35°. The measurements agree well with the theory prediction, shown in Fig. 3b, with the resonance wavelengths between the two differing by less than 2 nm. The measured Fano features are slightly broader than predicted, due to inhomogeneous broadening (since the measured data are averaged over many unit cells) and scattering loss introduced by disorders.

We extract the resonance lifetimes from the Fano features. By describing the guided resonances with temporal coupled-mode theory (CMT)[1], we find the reflectivity of the PhC slab to be

the thin-film reflectivity with the Fano features described by

$$f(\omega) = \frac{Q_{\mathrm{r}}^{-1}}{2i(1-\omega/\omega_0) + Q_{\mathrm{r}}^{-1} + Q_{\mathrm{nr}}^{-1}} \left(r_{\mathrm{slab}} - t_{\mathrm{slab}}\right), \tag{2}$$

where ω_0 is the resonance frequency, Q_{r} is the normalized radiative lifetime due to leakage into the free space, Q_{nr} is the normalized non-radiative lifetime, and r_{slab}, t_{slab} are the reflection and transmission coefficients of a homogeneous slab. The CMT setup is schematically illustrated in Fig. 3c, and a complete derivation is given in the Supplementary Information. The only unknowns in the CMT reflectivity expression are the resonance frequency and the lifetimes, which we obtain by fitting to the measured reflectivity spectrum. The fitted curves are shown in the bottom panel of Fig. 3c, and the obtained radiative Q_{r} is shown in Fig. 4a. At around 35°, Q_{r} reaches 1,000,000, near the instrument limit imposed by the resolution and signal-to-noise ratio, and in a good agreement with the values calculated from FDTD. We note that, the finite width and non-zero divergence of the excitation beam give rise to a spread of k points, leading to an upper bound of 10^{10} for the measured radiative Q_{r} (see Supplementary Information); in this experiment, this is not the limiting factor for the measured Q_{r}. In comparison, the non-radiative Q_{nr} is limited to about 10^4 which is due to loss from material absorption, disorder scattering, in-plane lateral leakage, and inhomogeneous broadening. Lastly, for validation, we repeated the same fitting procedure for the simulated reflectivity spectrum, and confirmed that consistent theoretical estimates of Q_{r} are obtained (Fig. 4b). These evidences quantitatively verify that we have observed the predicted bound state of light.

We have observed an optical state that remains perfectly confined even though there exist symmetry-compatible radiation modes in its close vicinity; this realizes the long sought-after idea

of trapping waves within the radiation continuum, without symmetry incompatibility[5–8,10–16]. The state has a high quality factor (implying low loss and large field enhancement), large area, and strong confinement near the surface, making it potentially useful for chemical/biological sensing, organic light emitting devices, and large-area laser applications. It also has wavevector and wavelength selectivity, making it suitable for optical filters, modulators, and waveguides. Furthermore, the ability to tune the maximal radiative Q_{r} from infinite to finite (Supplementary Fig. 2) is another unique property that may be exploited. Lastly, the fundamental principles of this state hold for any linear wave phenomenon, not just optics.

METHODS SUMMARY

Sample fabrication. The Si_3N_4 layer was grown by LPCVD on top of 6 μm thermally grown SiO_2 on a silicon wafer (LioniX), and subsequently coated with antireflection coating, a SiO_2 intermediate layer, and negative photoresist. The periodic PhC pattern was created with Mach-Zehnder interference lithography using a 325 nm He/Cd laser. Two orthogonal exposures defined the two-dimensional pattern. The interference angle was chosen for periodicity 336 nm, and the exposure time chosen for hole diameter 160 nm. After exposures, the sample was developed, and the pattern was transferred from photoresist to Si_3N_4 by reactive-ion etching; CHF_3/O_2 gas was used to etch SiO_2 and Si_3N_4, and He/O_2 gas was used to etch the antireflection coating.

Reflectivity measurement. The source was a supercontinuum laser (SuperK Compact, NKT Photonics) with divergence angle 6×10^{-4} radian and beam-spot width 2 mm on the PhC sample at normal incidence. A polarizer selected p-polarized light, which coupled with the TM_1 band. To create σ_z symmetry, the sample was immersed in a colorless liquid with index $n = 1.454$ at 740

nm (Cargille Labs). The sample was mounted on two perpendicular motorized rotation stages: one oriented the PhC to the Γ-X direction, while the other scanned the incident angle θ. The reflected beam was split into two and collected by two spectrometers, each with a resolution of 0.05 nm (HR4000, Ocean optics). Measurements were made every 0.5° from normal incidence to 60°.

---

1. Joannopoulos, J. D., Johnson, S. G., Winn, J. N. & Meade, R. D. *Photonic Crystals: Molding the Flow of Light* (Princeton University Press, 2008), 2 edn.

2. Lagendijk, A., van Tiggelen, B. & Wiersma, D. S. Fifty years of anderson localization. *Phys. Today* **62**, 24–29 (2009).

3. Plotnik, Y. *et al.* Experimental observation of optical bound states in the continuum. *Phys. Rev. Lett.* **107**, 183901 (2011).

4. Lee, J. *et al.* Observation and differentiation of unique high-q optical resonances near zero wave vector in macroscopic photonic crystal slabs. *Phys. Rev. Lett.* **109**, 067401 (2012).

5. Watts, M. R., Johnson, S. G., Haus, H. A. & Joannopoulos, J. D. Electromagnetic cavity with arbitrary q and small modal volume without a complete photonic bandgap. *Opt. Lett.* **27**, 1785–1787 (2002).

6. Marinica, D. C., Borisov, A. G. & Shabanov, S. V. Bound states in the continuum in photonics. *Phys. Rev. Lett.* **100**, 183902 (2008).

7. Molina, M. I., Miroshnichenko, A. E. & Kivshar, Y. S. Surface bound states in the continuum. *Phys. Rev. Lett.* **108**, 070401 (2012).

8. Hsu, C. W. *et al.* Bloch surface eigenstates within the radiation continuum. *Light: Science & Applications* **2**, e84 (2013). doi:10.1038/lsa.2013.40.

9. Hislop, P. D. & Sigal, I. M. *Introduction to Spectral Theory: with Applications to Schrödinger Operators* (Springer Verlag, 1996).

10. von Neumann, J. & Wigner, E. Über merkwürdige diskrete eigenwerte. *Phys. Z.* **30**, 465–467 (1929).

11. Stillinger, F. H. & Herrick, D. R. Bound states in the continuum. *Phys. Rev. A* **11**, 446–454 (1975).

12. Friedrich, H. & Wintgen, D. Interfering resonances and bound states in the continuum. *Phys. Rev. A* **32**, 3231–3242 (1985).

13. Zhang, J. M., Braak, D. & Kollar, M. Bound states in the continuum realized in the one-dimensional two-particle hubbard model with an impurity. *Phys. Rev. Lett.* **109**, 116405 (2012).

14. Porter, R. & Evans, D. Embedded rayleigh-bloch surface waves along periodic rectangular arrays. *Wave Motion* **43**, 29 – 50 (2005).

15. Linton, C. M. & McIver, P. Embedded trapped modes in water waves and acoustics. *Wave Motion* **45**, 16 (2007).

16. Krüger, H. On the existence of embedded eigenvalues. *J. Math. Anal. Appl.* **395**, 776 (2012).

17. Taflove, A. & Hagness, S. C. *Computational electrodynamics: the finite-difference time-domain method* (Artech House, 2005), 3 edn.

18. Johnson, S. G. & Joannopoulos, J. D. Block-iterative frequency-domain methods for maxwell's equations in a planewave basis. *Opt. Express* **8**, 173–190 (2001).

19. Fan, S. & Joannopoulos, J. D. Analysis of guided resonances in photonic crystal slabs. *Phys. Rev. B* **65**, 235112 (2002).

20. Liu, V. & Fan, S. S^4 : A free electromagnetic solver for layered periodic structures. *Comput. Phys. Commun.* **183**, 2233 – 2244 (2012).

Supplementary Information is available in the online version of the paper.

Acknowledgements We thank Ling Lu, Ofer Shapira, and Yichen Shen for stimulating discussions. This work was partially supported by the Army Research Office through the Institute for Soldier Nanotechnologies under Contract No. W911NF-07-D0004. B.Z., J.L. (fabrication), and M.S. were partially supported by S3TEC, an Energy Frontier Research Center funded by the U.S. DOE under Grant No. DE-SC0001299. S.-L.C. and J.L. were also partially supported by the Materials Research Science and Engineering Centers of the NSF under Grant No. DMR-0819762.

Author Contributions C.W.H., B.Z., S.-L.C., J.D.J., and M.S. conceived the idea of this study. C.W.H. performed numerical simulations. C.W.H. and B.Z. conducted the measurement and analysis. J.L. fabricated the sample. S.G.J. proposed the Fourier-coefficient explanation. M.S. and J.D.J. supervised the project. C.W.H. wrote the paper with input from all authors.

Author Information Reprints and permissions information is available at www.nature.com/reprints. The authors declare no competing financial interests. Correspondence and requests for materials should be addressed to C.W.H. (email: cwhsu@mit.edu).

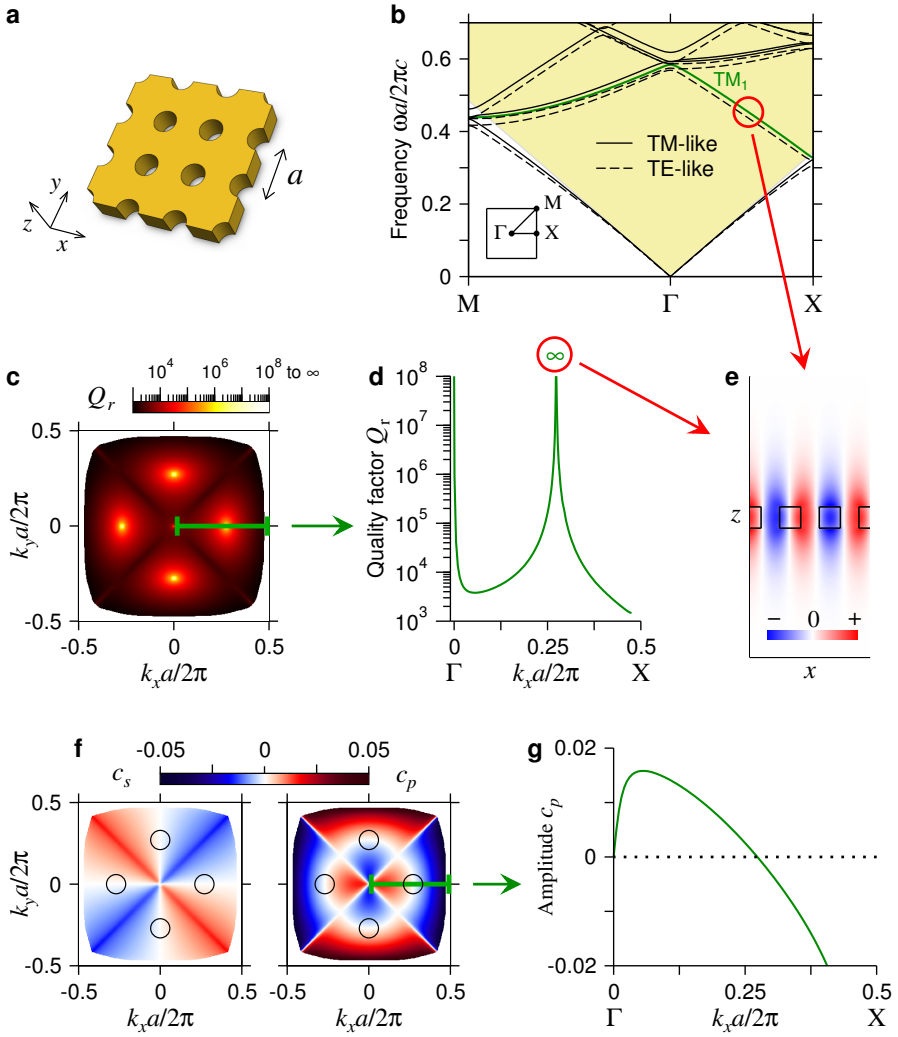

Figure 1: **Theory predictions. a,** Schematic of the photonic crystal (PhC) slab. **b,** Calculated band structure. Yellow shaded area indicates light cone of the surrounding medium, where there is a continuum of radiation modes in free space. The trapped state is marked with a red circle, and the TM_1 band is marked with a green line. Inset shows the first Brillouin zone. **c, d,** Normalized radiative lifetime Q_r of the TM_1 band calculated from FDTD, with values along the Γ-X direction shown in **d**. Below the light cone there is no radiation mode to couple to (*i.e.* total internal reflection), so Q_r is infinite. But at discrete points inside the light cone, Q_r also goes to infinity. **e,** Electric-field profile E_z of the trapped state, plotted on the $y = 0$ slice. **f, g,** Amplitudes of the s- and p-polarized outgoing planewaves for the TM_1 band, with c_p along the Γ-X direction shown in **g**. Black circles in **f** indicate k points where both c_s and c_p are zero.

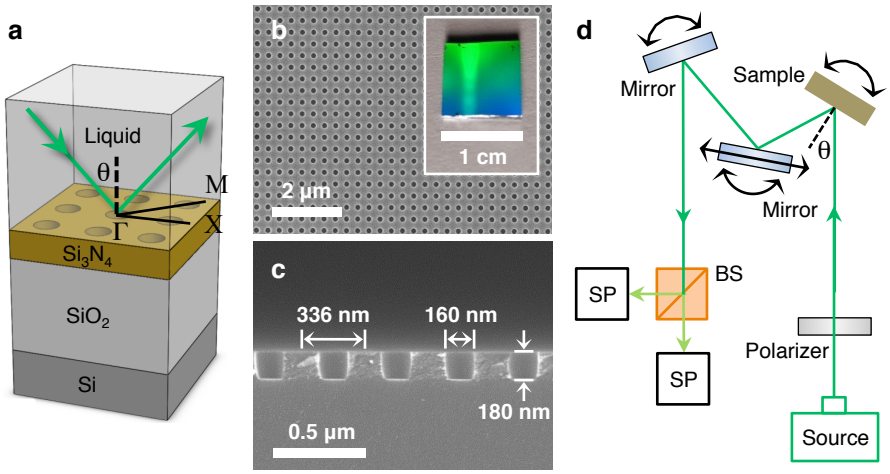

Figure 2: **Fabricated PhC slab and the measurement setup. a** Schematic layout of the fabricated structure. The device is immersed in a liquid, index-matched to silica at 740 nm wavelength. **b, c,** SEM images of the structure in top view and side view. Inset of **b** shows an image of the whole PhC. **d,** Schematic of the setup for reflectivity measurements. BS, beamsplitter; SP, spectrometer.

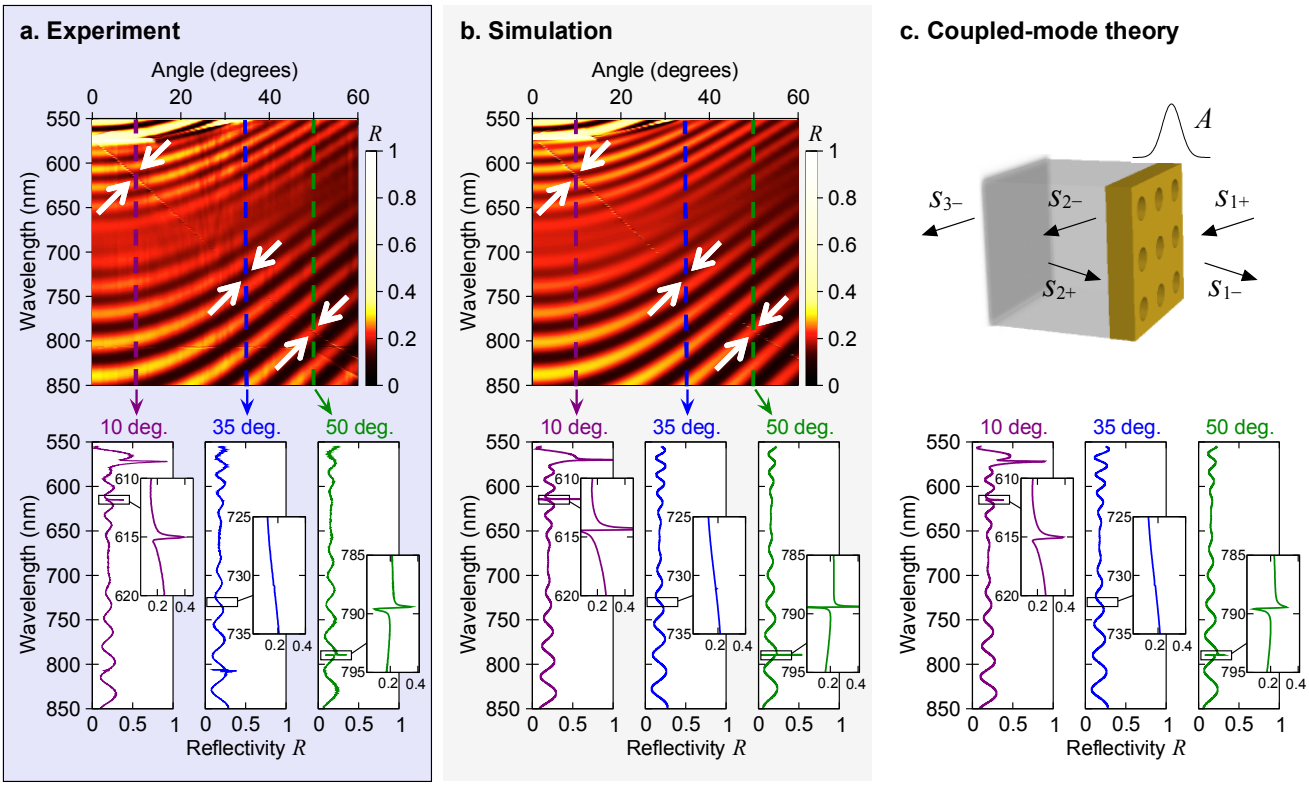

Figure 3: **Detection of resonances from reflectivity data. a,** Experimentally measured specular reflectivity for p-polarized light along Γ-X. The crucial feature of interest is the resonance, which shows up as a thin faint line (emphasized by white arrows) extending from the top-left corner of the top panel to the bottom-right corner. Disappearance of the resonance feature near 35° indicates a trapped state with no leakage. Bottom panel shows slices at three representative angles, with close-ups near the resonance features. **b,** Calculated p-polarized specular reflectivity using the rigorous coupled-wave analysis (RCWA) method[20] with known refractive indices and measured layer thickness. **c,** Top: schematic for the scattering process in temporal coupled-mode theory (CMT), which treats the resonance A and the incoming/outgoing planewaves $s_{m\pm}$ as separate entities weakly coupled to each other. Bottom: reflectivity given by the analytical CMT expression; the resonance frequency and lifetimes, which are the only unknowns in the CMT expression, are fitted from the experimental data in **a**.

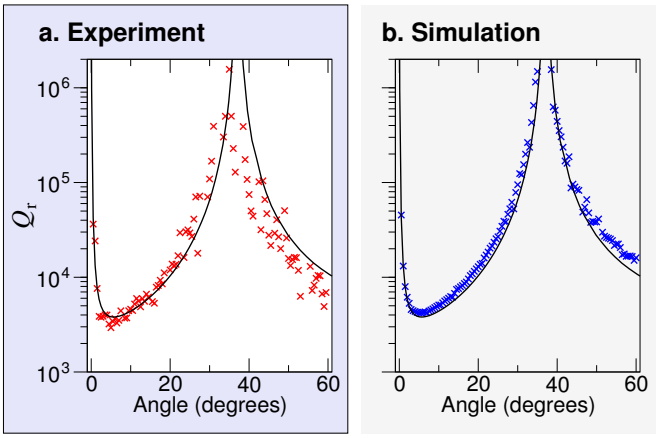

Figure 4: **Quantitative evidence on the disappearance of leakage. a, b,** Normalized radiative lifetime Q_{r} extracted from the experimentally-measured reflectivity spectrum (**a**) and the RCWA-calculated reflectivity spectrum (**b**). Black solid line shows prediction from FDTD.

SUPPLEMENTARY EQUATIONS

Coupled-mode theory and fitting. In temporal coupled-mode theory (CMT), the field A of the resonance and fields $s_{m\pm}$ of the incoming/outgoing planewaves are considered separate entities that are weakly coupled to each other through their spatial overlaps[1,21]. A schematic illustration is given in Fig. 3c of the main text. The resonance decays with a radiative-decay lifetime τ_{r} from leakage into the outgoing planewaves, and a non-radiative-decay lifetime τ_{nr} from material absorption and disorder scattering. As we will see, the effect of τ_{nr} is to broaden the resonance feature in the reflectivity spectrum; therefore it also heuristically accounts for the inhomogeneous broadening in the measured reflectivity data. Incoming planewaves excite the resonance with coupling coefficients denoted by κ_1 and κ_2. Thus we have

$$\frac{dA}{dt} = \left(-i\omega_0 - \frac{1}{\tau_{\mathrm{r}}} - \frac{1}{\tau_{\mathrm{nr}}}\right) A + \kappa_1 s_{1+} + \kappa_2 s_{2+}. \tag{1}$$

The planewaves on the two sides of the slab couple to each other through a direct scattering process, with transmission and reflection coefficients t_{slab} and r_{slab}. The resonance decays into the outgoing planewaves, with coupling coefficients denoted by d_1 and d_2. Therefore,

$$s_{1-} = r_{\mathrm{slab}} s_{1+} + t_{\mathrm{slab}} s_{2+} + d_1 A, \tag{2}$$

$$s_{2-} = t_{\mathrm{slab}} s_{1+} + r_{\mathrm{slab}} s_{2+} + d_2 A. \tag{3}$$

Lastly, the reflection at the silica-silicon interface (with coefficient r_{23}) and the propagation inside the silica layer impose that

$$s_{2+} = e^{2i\beta h_2} r_{23} s_{2-} \tag{4}$$

where $\beta = \sqrt{n_{\mathrm{SiO_2}}^2 \omega^2/c^2 - |\mathbf{k}|^2}$ is the propagation constant in the silica layer, and h_2 is the layer's thickness. The normalization of the field amplitudes is chosen such that $|A|^2$ is the energy stored in the resonance, and $|s_{m\pm}|^2$ is the power carried by the incoming or outgoing planewaves.

Now, assume $e^{-i\omega t}$ time dependence for the resonance amplitude A. Solving equations (1–4) as a system of linear equations, we obtain

$$\frac{s_{1-}}{s_{1+}} = r_{\mathrm{slab}} + \frac{d_1\kappa_1}{i(\omega_0-\omega) + \tau_{\mathrm{r}}^{-1} + \tau_{\mathrm{nr}}^{-1}} + \frac{\left[t_{\mathrm{slab}} + \frac{d_1\kappa_2}{i(\omega_0-\omega)+\tau_{\mathrm{r}}^{-1}+\tau_{\mathrm{nr}}^{-1}}\right]\left[t_{\mathrm{slab}} + \frac{d_2\kappa_1}{i(\omega_0-\omega)+\tau_{\mathrm{r}}^{-1}+\tau_{\mathrm{nr}}^{-1}}\right]}{e^{-2i\beta h_2} r_{23}^{-1} - r_{\mathrm{slab}} - \frac{d_2\kappa_2}{i(\omega_0-\omega)+\tau_{\mathrm{r}}^{-1}+\tau_{\mathrm{nr}}^{-1}}} \tag{5}$$

which gives us the overall reflectivity. This expression can be simplified, as follows. First, σ_z mirror-flip symmetry of the PhC slab requires fields of the resonance to be either even or odd in z, and so $d_2 = \pm d_1$. Secondly, energy conservation requires that in the absence of input power ($s_{1+} = s_{2+} = 0$), the energy dissipated through radiative decay must be carried away by s_{1-} and s_{2-}; this leads to $|d_1|^2 = 1/\tau_{\mathrm{r}}$. Thirdly, inversion symmetry I and σ_z mirror symmetry yields

$I\sigma_z = C_2$ rotational symmetry about the plane normal, and a combination of time reversal symmetry and C_2 symmetry leads to $r_{\text{slab}}d_1^* + t_{\text{slab}}d_2^* + d_1 = 0$ (refs. 8, 22). A combination of these facts yields

$$d_1^2 = -\frac{1}{\tau_{\text{r}}}(r_{\text{slab}} \pm t_{\text{slab}}). \tag{6}$$

Lastly, the coupling coefficients for the incoming and for the outgoing waves are actually the same under energy conservation and time reversal requirements[1,21,22], *i.e.* $d_1 = \kappa_1$ and $d_2 = \kappa_2$. With these known properties, we can write the overall reflectivity as

$$R = \left|\frac{s_{1-}}{s_{1+}}\right|^2 = \left|r_{\text{slab}} - f(\omega) + \frac{[t_{\text{slab}} \mp f(\omega)]^2}{e^{-2i\beta h_2}r_{23}^{-1} - r_{\text{slab}} + f(\omega)}\right|^2 \tag{7}$$

with

$$f(\omega) = \frac{Q_{\text{r}}^{-1}}{2i(1-\omega/\omega_0) + Q_{\text{r}}^{-1} + Q_{\text{nr}}^{-1}}\left(r_{\text{slab}} \pm t_{\text{slab}}\right), \tag{8}$$

where $Q_{\text{r}} = \omega_0\tau_{\text{r}}/2$ and $Q_{\text{nr}} = \omega_0\tau_{\text{nr}}/2$ are the normalized lifetimes. We fit the experimentally measured reflectivity spectrum with this expression to extract the lifetime of the resonances.

We note that, the only unknowns in this reflectivity expression are the resonance frequency and the lifetimes: r_{23} is given by the Fresnel equations, and r_{slab}, t_{slab} can be approximated as the reflection and transmission coefficients of a homogeneous slab whose permittivity is equal to the spatial average of the PhC slab[19,22].

In the absence of $f(\omega)$, equation (7) reduces to the expression for multi-layer thin-film reflectivity. Therefore the Fano features are completely captured by $f(\omega)$. From equation (8), we see that the width of the Fano feature is proportional to $Q_{\text{r}}^{-1} + Q_{\text{nr}}^{-1}$, while the height of the feature grows with Q_{r}^{-1}. This confirms our intuitive understanding that, when the resonance becomes a bound state ($Q_{\text{r}} = \infty$), it decouples from the far field, and the Fano feature disappears.

It is straightforward to generalize this CMT expression to include multiple resonances in the spectrum; same derivation shows that we can simply replace $f(\omega)$ in equation (7) with a summation $\sum_j f^{(j)}(\omega)$ for different resonances labeled by j. Each resonance has its resonant frequency and lifetimes that are to be determined from the fitting. Lastly, we note that the $\pm$ signs relate to how the resonance fields transform under mirror flips in z. When the electric field is used to determine the phase of A and $s_{m\pm}$, we should read the upper signs for TE-like modes, lower signs for TM-like modes.

SUPPLEMENTARY DISCUSSION

Effects of non-perfect excitation beam Our analysis so far assumes excitation with a perfect planewave. However, some care must be taken with the Gaussian beam from the supercontinuum source. First, the beam spot has a diameter of 2 mm at normal incidence, so the excited mode has a finite lateral size of $L \approx 2$ mm. This finite-sized mode consists of a spread of k points, with $\delta k_{\rm mode} \approx 2\pi/L \approx (2\times10^{-4})(2\pi/a)$. Second, the beam has a divergence angle of $\delta\theta \approx 6\times10^{-4}$ radian, so the source also has a spread of k points, with $\delta k_{\rm source} \approx (2\pi/\lambda)\delta\theta \approx (3\times10^{-4})(2\pi/a)$. The measured radiative loss will be the averaged value within this spread of k points.

The outgoing-wave amplitude goes through zero linearly (see Fig. 1g of the main text), so the outgoing power goes as $(\Delta k)^2$ near the embedded bound states, where $\Delta k = |\mathbf{k}-\mathbf{k}_0|$ is distance from the special k point, $\mathbf{k}_0$. Specifically, FDTD simulations show that near the special trapped state studied in this paper, $Q_{\rm r} \approx 100/(\Delta k a/2\pi)^2$. In a circular area with diameter δk, the effective $Q_{\rm r}$ will be $800/(\delta k a/2\pi)^2$, which is around 10^{10} for the k-point spread due to the beam. This sets the upper limit on the $Q_{\rm r}$ we can obtain with our source.

References

21. Haus, H. A. *Waves and Fields in Optoelectronics* (Prentice-Hall, 1984).

22. Fan, S., Suh, W. & Joannopoulos, J. D. Temporal coupled-mode theory for the Fano resonance in optical resonators. *J. Opt. Soc. Am. A* **20**, 569 (2003).

SUPPLEMENTARY FIGURES

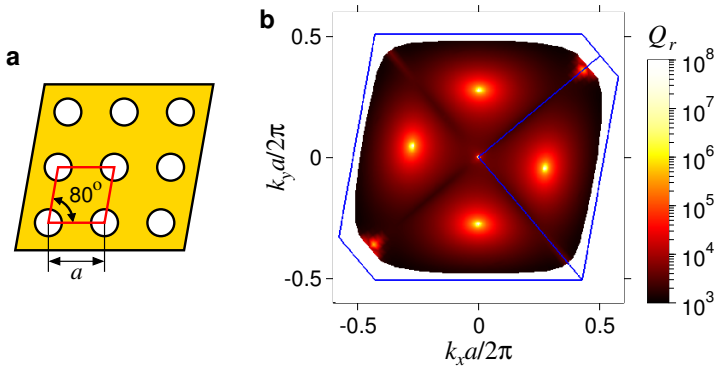

Supplementary Figure 1: **Existence of infinite-Q_{r} state in a rhombic-lattice photonic crystal slab. a,** The lattice viewed from above, with the unit cell framed in red. **b,** Lifetime of the TM_1 band. Compared to the square-lattice case (Fig. 1c in main text), the special trapped states simply shift to different k points. Blue lines indicate the boundary of the first Brillouin zone and the irreducible Brillouin zone. On a rhombic lattice, C_4 rotational symmetry is broken, but the structure still has inversion symmetry and C_2 rotational symmetry.

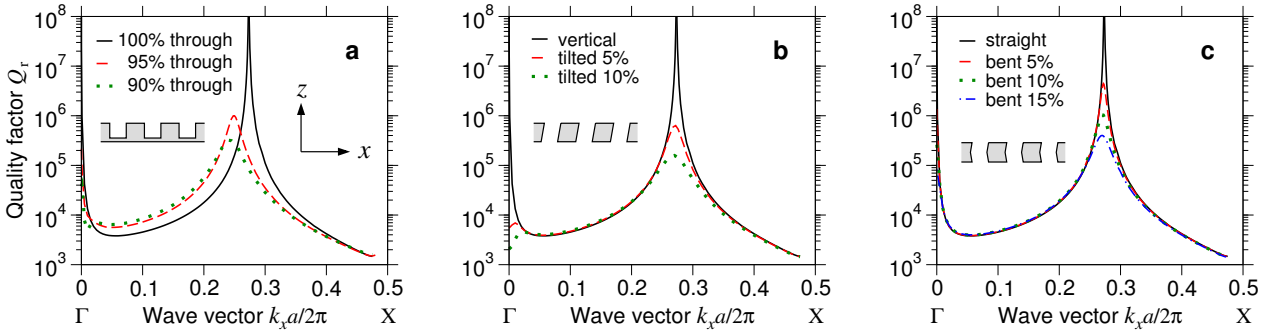

Supplementary Figure 2: **Dependence of the TM_1 band lifetime on perturbations that break inversion symmetry I or mirror-flip symmetry σ_z. a,** Square-lattice photonic crystal slab with cylindrical holes that are not etched through the entire slab. Both I and σ_z are broken. **b,** Slab with tilted cylindrical holes. σ_z is broken but I is intact. **c,** Slab with cylindrical holes that are bent in the middle. I is broken but σ_z is intact.